Investigation of the Summer Climate of the Contiguous United States and Mexico Using the Regional Atmospheric Modeling System (RAMS). Part II: Model Climate Variability

CHRISTOPHER L. CASTRO*

Department of Atmospheric Science, Colorado State University, Fort Collins, Colorado

ROGER A. PIELKE SR.

Cooperative Institute for Research in Environmental Sciences, Program in Atmospheric and Oceanic Sciences, University of Colorado, Boulder, Colorado

JIMMY O. ADEGOKE

Laboratory for Climate Analysis and Modeling, Department of Geosciences, University of Missouri—Kansas City, Kansas City, Missouri

SIEGFRIED D. SCHUBERT AND PHILLIP J. PEGION

NASA Goddard Laboratory for Atmospheres, Greenbelt, Maryland

(Manuscript received 22 November 2005, in final form 27 November 2006)

ABSTRACT

Summer simulations over the contiguous United States and Mexico with the Regional Atmospheric Modeling System (RAMS) dynamically downscaling the NCEP–NCAR Reanalysis I for the period 1950–2002 (described in Part I of the study) are evaluated with respect to the three dominant modes of global SST. Two of these modes are associated with the statistically significant, naturally occurring interannual and interdecadal variability in the Pacific. The remaining mode corresponds to the recent warming of tropical sea surface temperatures. Time-evolving teleconnections associated with Pacific SSTs delay or accelerate the evolution of the North American monsoon. At the period of maximum teleconnectivity in late June and early July, there is an opposite relationship between precipitation in the core monsoon region and the central United States. Use of a regional climate model (RCM) is essential to capture this variability because of its representation of the diurnal cycle of convective rainfall. The RCM also captures the observed long-term changes in Mexican summer rainfall and suggests that these changes are due in part to the recent increase in eastern Pacific SST off the Mexican coast. To establish the physical linkage to remote SST forcing, additional RAMS seasonal weather prediction mode simulations were performed and these results are briefly discussed. In order for RCMs to be successful in a seasonal weather prediction mode for the summer season, it is required that the GCM provide a reasonable representation of the teleconnections and have a climatology that is comparable to a global atmospheric reanalysis.

1. Introduction

This paper is the second in a series investigating the summer climate of the contiguous United States and Mexico with a regional climate model (RCM). The previous paper (Castro et al. 2007, hereafter Part I) described the climatological behavior of 53 years of summer simulations with the Regional Atmospheric Modeling System (RAMS) dynamically downscaling the National Centers for Environmental Prediction–National Center for Atmospheric Research (NCEP–NCAR) reanalysis (Kalnay et al. 1996) in a seasonal weather simulation mode. It was shown that the RCM added value to the representation of summer climate beyond the driving global reanalysis (GR) and compared favorably with the North American Regional Reanalysis (NARR; Mesinger et al. 2006). The key improvement

* Current affiliation: Department of Atmospheric Sciences, The University of Arizona, Tucson, Arizona.

Corresponding author address: Dr. Christopher L. Castro, Department of Atmospheric Sciences, The University of Arizona, Physics and Atmospheric Sciences Bldg., Rm. 520, 1118 East Fourth Street, Tucson, AZ 85721-0081.
E-mail: castro@atmo.arizona.edu

DOI: 10.1175/JCLI4212.1

of the summer climate in the RCM is the presence of the diurnal cycle of convective rainfall due to the enhanced representation of the land surface boundary. This diurnal cycle governs the transitions associated with the evolution of the North American monsoon. The lower frequency modes of convective rainfall acted at a distance from elevated terrain. Here the RCM results are considered with respect to global modes of SST. The present investigation aims primarily to demonstrate the value added of a RCM in representing long-term climate variability in the summer season for the region. The potential utility of a RCM for seasonal weather prediction for the summer season will also be briefly discussed. A description of the RAMS model and setup for the RCM simulations can be found in section 2 of Part I.

There are numerous observational analyses that suggest a strong connection between North American summer climate and Pacific SSTs. While the Atlantic may also play a role (e.g., Sutton and Hodson 2005), consideration of Pacific SST variability will be the focus of the analysis of the RCM results here. The study by Castro et al. (2001) shows a statistically significant relationship between tropical and North Pacific SST and the evolution of the North American monsoon system (NAMS). The strongest relationship to Pacific SSTs occurs at monsoon onset. These conclusions of Castro et al. (2001) are in agreement with similar observational studies, including Ting and Wang (1997), Hu and Feng (2001, 2002), Englehart and Douglas (2002, 2003), Higgins et al. (1999), Mo and Paegle (2000), and Higgins and Shi (2001). Also, the position of the monsoon ridge for wet and dry monsoons in the U.S. Southwest is generally in agreement with Carleton et al. (1990) and Cavazos et al. (2002).

The likely explanation for the connection of North American summer climate to Pacific SSTs is via a midlatitude atmospheric teleconnection response, as demonstrated in idealized modeling studies by Trenberth and Branstator (1992), Lau and Peng (1992), and Newman and Sardeshmukh (1998). The latter two studies conclude that the teleconnection response is maximized in late spring to early summer and related to forcing in the central and west Pacific. The time dependence of the teleconnection response is most likely related to the climatological evolution of the East Asian jet across the Pacific, as advection of the vorticity gradient creates an effective Rossby wave source in the midlatitudes (e.g., Sardeshmukh and Hoskins 1988).

Atmospheric general circulation models (GCMs) have also been employed to investigate the boreal summer climate and its relationship to sea surface temperature. Hoerling and Kumar (2003) reproduced the atmospheric circulation conditions associated with the recent 1998–2002 drought in North America by varying SSTs in the tropical Pacific. Schubert et al. (2002) specifically tested the hypothesis that variations in the dominant modes of global SST produce global teleconnections in boreal summer. They executed boreal summer ensemble simulations with the NASA Seasonal-to-Interannual Prediction Project (NSIPP-1) GCM forced with the dominant modes of global SST (for the period 1980–99) superimposed on the SST climatology. These modes are related to two global teleconnection patterns that are symmetric with respect to the equator in both observations and GCM simulations when a 3-month [June–August (JJA)] mean is considered. In a similar and more recent GCM study with the same model, Schubert et al. (2004) have related long-term (greater than 6 yr) rainfall variability to a pan-Pacific mode in SST and concluded it is the tropical part of the SST anomalies that has the most influence on the extratropical teleconnection.

The outline for the paper is as follows. Section 2 confirms that the original SST modes obtained by Schubert et al. (2002) represent the significant time varying modes of global SST. Once this fact is established, composites for the 53-yr RCM are constructed corresponding to these modes. Section 3 establishes that the summer teleconnection patterns associated with these modes vary in time, as in Castro et al. (2001). Section 4 demonstrates how the RCM adds value in representing climate variability associated with the SST modes. A discussion and summary are given in sections 5 and 6, respectively.

2. Extension of the Schubert et al. global SST analysis

The original rotated EOF analysis (REOF; Richman 1986) of Schubert et al. (2002) on boreal summer SST is extended using the data of Reynolds and Smith (1994) to the period 1950–2000. The intent of the analysis here is simply to construct statistical composites to match those of Schubert et al. (2002), not reinvent any SST modes or indices already widely used and documented. Shown in Figs. 1 and 2 are the first three REOFs of the 1950–2000 period and the normalized principal component (PC) time series. The REOF 1 and REOF 3 patterns match the two modes considered in Schubert et al. and are labeled Pacific "Variability Mode" 1 and 2, respectively, since their variation is confined there. REOF 2 appears as a new mode in the longer record, and it is labeled as the Tropical SST "Warming Mode" since it is associated with a global increase in tropical SST since the early 1980s of 0.25–0.5 K.

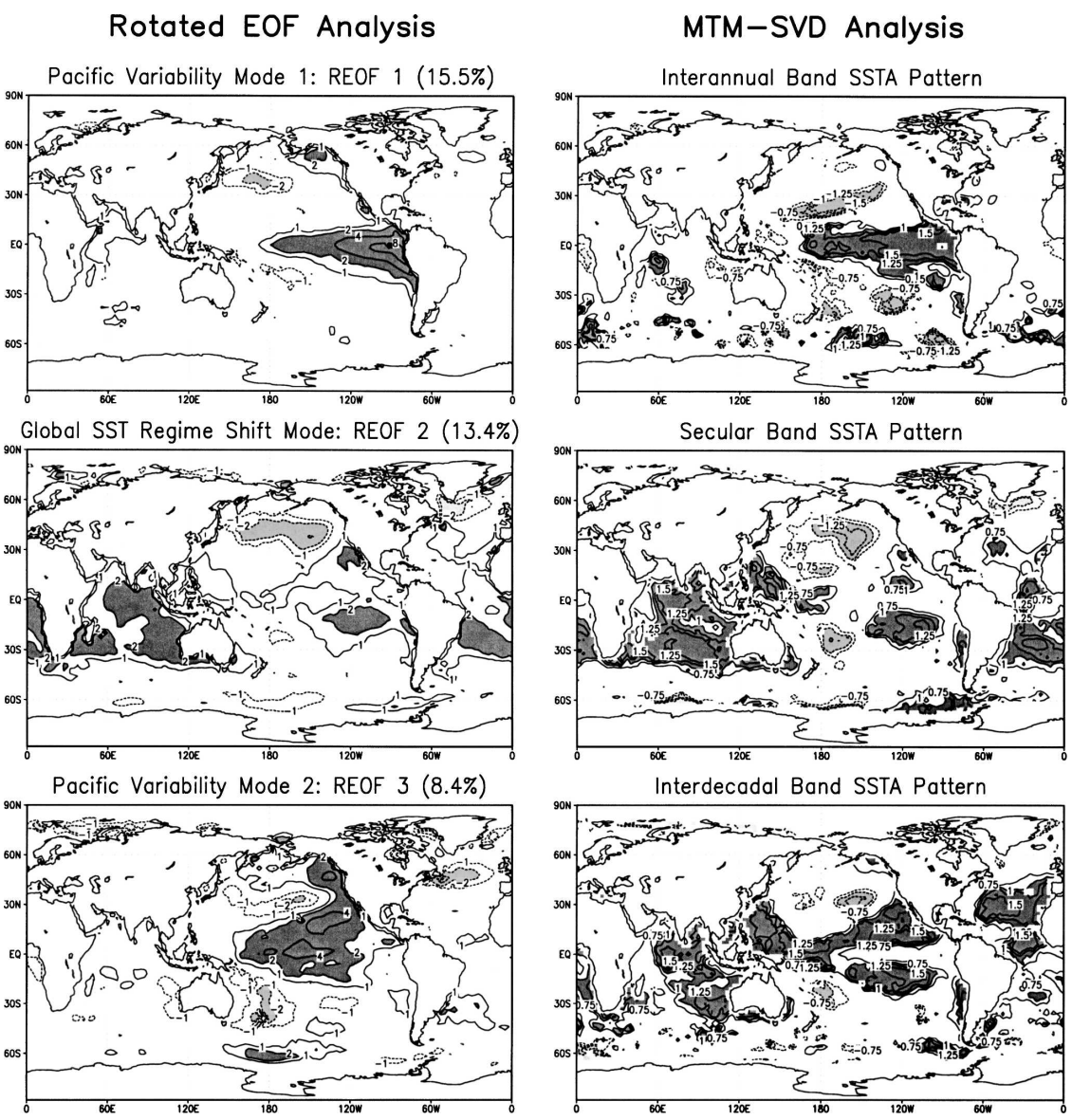

FIG. 1. (left) The first three REOFs of global SST for the period 1950–2000. For REOF patterns units are arbitrary and contour interval is one unit. Values greater (less) than 2 (−2) are shaded dark (light). (right) The corresponding (in phase) normalized SSTA associated with interannual, secular, and interdecadal bands from the MTM–SVD analysis, referenced to the eastern tropical Pacific (0°, 160°W). Values greater (less) than 1 (−1) shaded dark (light). Contour interval is 0.25 units.

These REOFs are not statistically significant by standard tests of eigenvalue separation (e.g., North et al. 1982). To establish that these patterns reflect significant time variation in global SST, a multitaper frequency domain, singular value decomposition (MTM–SVD) approach is used. The specific details and references for the method are included in the appendix. MTM–SVD analysis allows for the detection and reconstruction of quasi-oscillatory spatiotemporal climate signals that exhibit episodes of spatially correlated behavior and has demonstrated utility in a wide variety of geophysical applications (Rajagopalan et al. 1998). It produces 1) a local fractional variance (LFV) spectrum of the principal eigenmode; 2) statistical confidence intervals for the LFV spectrum; and 3) reconstructed SST anomaly (SSTA) patterns corresponding to the significant time-varying modes. Figure 3 shows the principal eigenmode LFV spectrum of boreal summer SSTA for the period 1950–2000. Two significant spectral peaks appear, an interannual band (3–4 yr) and an interdecadal band

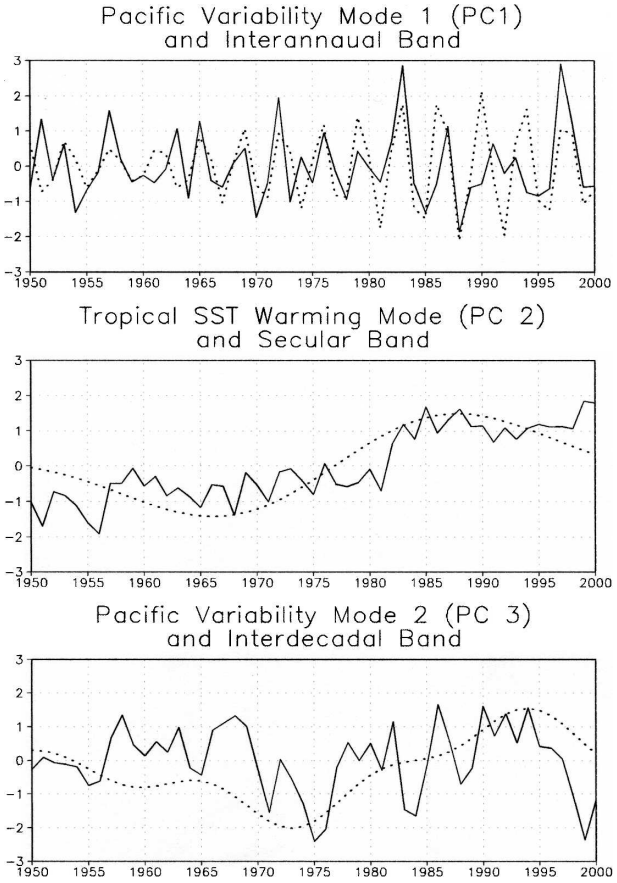

FIG. 2. Normalized PC time series (1950–2000) for boreal summer SST modes in Fig. 1 (solid line) and corresponding time series of normalized SSTA associated with interannual, secular, and intedecadal bands from MTM–SVD analysis (dotted line) referenced to the eastern tropical Pacific (0°, 160°W).

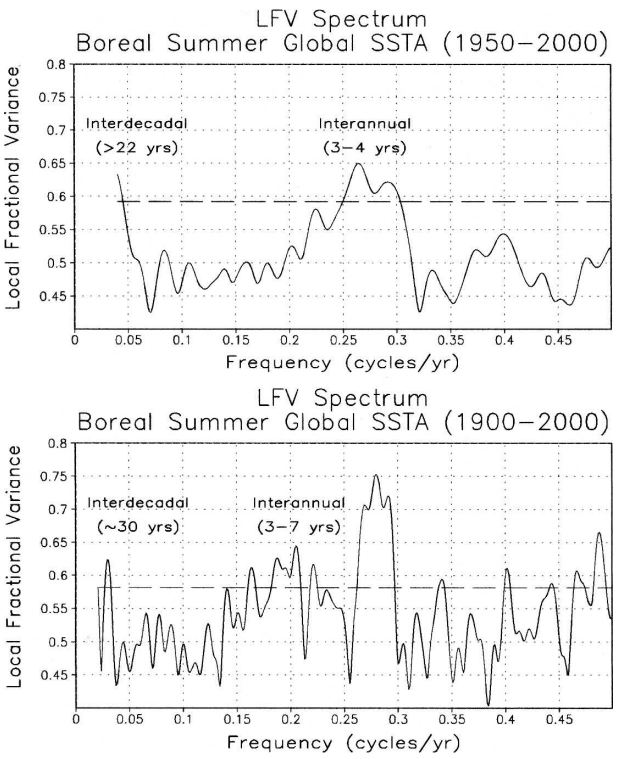

FIG. 3. Principal eigenmode local fractional variance spectrum of boreal summer global SST for the (top) 1950–2000 period from data of Reynolds and Smith (1994) and (bottom) 1900–2000 period from the data of Kaplan et al. (1998). Dashed line indicates statistical significance at the 99% level. Significant spectral peaks and their approximate time scale are indicated.

(greater than 22 yr). Identical analysis of the SST data of Kaplan et al. (1998) for the period 1900–2000, also shown in Fig. 3, confirms that the decadal variability appears as a distinct spectral peak. The right-hand side of Fig. 1 shows the (in phase) SSTA associated with the significant spectral peaks in Fig. 3, referenced to the central tropical Pacific (0°, 160°W). Their normalized time series is also plotted with the PCs for comparison in Fig. 2. The interannual, intedecadal, and secular band SSTAs broadly correspond to the dominant modes obtained in the REOF analysis. The greatest discrepancy occurs for REOF 3, particularly outside the North Pacific.

The preceding analysis confirms that two of the dominant REOFs reflect the significant time-varying modes of Pacific SST. Pacific variability mode 1 is clearly ENSO. As in Zhang et al. (1997), Pacific variability mode 2 approximately reflects decadal variability, and its variation matches cycles of drought in the central United States (e.g., McKee et al. 1999; Castro et al. 2001), including the most recent one (Hoerling and Kumar 2003; Pielke et al. 2005). It is probably not appropriate to refer to Pacific variability mode 2 as the Pacific decadal oscillation (PDO) as defined in Mantua et al. (1997) since the PDO is defined regionally within the North Pacific. The physical mechanisms for decadal variability in SST are not clear and not the subject of this paper. Hypothesized mechanisms include atmospheric forcing due to tropical SST variability (e.g., Alexander et al. 2002; Karspeck et al. 2004; Seager et al. 2004), stochastic variability (e.g., Deser et al. 2003; Chiang and Vimont 2004), internal ocean dynamics (e.g., Philander and Gu 1997), or some combination thereof (e.g., Schneider and Cornuelle 2005). In any case, both of these modes reflect natural variability in the climate system. Though the "Tropical Warming Mode" is not distinctly separated from the interdecadal mode of SSTA in Fig. 3, it deserves to be treated as a separate and distinct entity because 1) the recent warming in tropical SSTs has been documented and considered in prior studies (e.g., Levitus et al. 2000; Kumar et

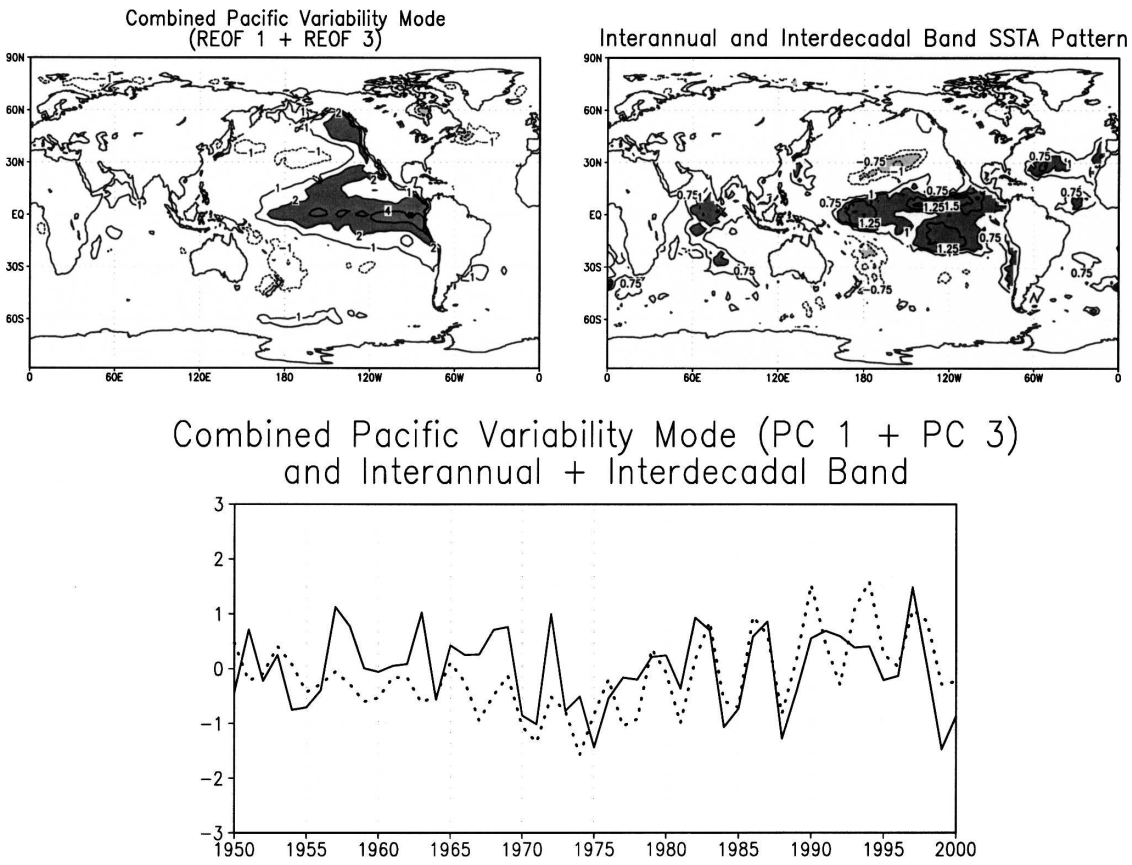

FIG. 4. As in Figs. 1 and 2 but for the combined Pacific variability mode and the combination of interannual and interdecadal band SSTA.

al. 2004) and 2) it has been asserted that the warming may be due to anthropogenic climate change (Barnett et al. 2001, 2005; Hansen et al. 2005). The discussion in section 5 will provide further substantiation for the consideration of this mode based on the results presented in sections 3 and 4. Given the conclusion in Castro et al. (2001) that the most coherent summer climate patterns in western North America occur when a combined index of tropical and North Pacific SSTs is substantially high or low, Pacific variability modes 1 and 2 and the interannual and interdecadal bands of SSTA from the MTM–SVD analysis are averaged together (Fig. 4). Henceforth this mode is referred to as the "Combined Pacific Variability Mode." It combines the interannual and interdecadal variability in Pacific SSTs and is very similar to the pan-Pacific mode of Schubert et al. (2004). This mode will be used to consider the RCM simulation results for the observed years in section 4.

Each individual time series corresponding to the modes just described is used to construct a positive and negative composite of years (see Tables 1–4). The positive and negative composites consider years that exceed half a standard deviation of their given (PC) time series. Though not included in the SST analysis, 2001 and 2002 are considered as being in the negative phase of Pacific variability mode 2 because of the aforementioned drought conditions in the central United States. The positive composite of the tropical SST warming mode is just the last 21 years of the record. Local significance of anomalies above the 90% level in the proceeding sections is determined by a two-tailed t test that considers the years within a given composite minus the remaining years. As in Livezey and Chen (1983), field significance (f) is determined by a Monte Carlo procedure in which the subsets of years are randomly resampled 1000 times. The figures depicting results in sections 3 and 4 show the positive minus negative phase of the given composite divided by two.

3. Observed time-evolving SST-associated teleconnection patterns

The difference in the 30-day average NCEP–NCAR Reanalysis 500-mb height field about the date and corresponding statistical significance were calculated for the composites in Tables 1–3. Results for Pacific vari-

TABLE 1. Years in the 1950–2002 period included in positive and negative composites for Pacific variability mode 1.

Negative	Positive
1950	1951
1954	1953
1955	1957
1964	1963
1967	1965
1970	1969
1973	1972
1978	1976
1985	1982
1988	1983
1989	1987
1994	1991
1995	1997
1996	1998
1999	
2000	

ability mode 1, Pacific variability mode 2, and the tropical SST warming mode are shown in Figs. 5, 6, and 7, respectively, for the area that includes the tropical and North Pacific Ocean and North America. For convenience and comparison, the days are chosen to coincide with those of Castro et al. (2001, their Figs. 3 and 4). Figures 5 and 6 show that the Pacific variability modes are associated with wave trains across the Pacific, consistent with the idealized modeling studies mentioned in the introduction. The Pacific variability mode-1 teleconnection has a significant center of action in the northern Rocky Mountains in early July. The stronger and more significant teleconnection response is associated with Pacific variability mode 2. This teleconnection peaks slightly later (early to mid-July) over the contiguous United States in the northern Great Plains. Both teleconnections are field significant at about the 90% level and above in the early part of the summer. Any significant relationships in the 500-mb height field over the contiguous United States disappear by August, corresponding to a decrease in the strength of the East Asian jet in the Pacific (see Fig. 5 of Castro et al. 2001). A similar pattern of time-dependent midlatitude height anomalies appears in the shorter 1980–99 record (not shown), confirming that the results are not an artifact of the sample size. At the period of "maximum teleconnectivity" in July the patterns associated with Pacific variability modes 1 and 2 are distinct. The centers of action over the contiguous United States on 4 July, for example, are approximately in quadrature.

TABLE 2. As in Table 1 but for Pacific variability mode 2.

Negative	Positive
1955	1957
1956	1958
1971	1961
1973	1963
1974	1966
1975	1967
1976	1968
1983	1969
1984	1978
1988	1980
1998	1982
1999	1986
2000	1987
2001	1990
2002	1991
	1992
	1993
	1994
	1995

TABLE 3. As in Table 1 but for the tropical SST warming mode.

Negative	Positive
1950	1982
1951	1983
1952	1984
1953	1985
1954	1986
1955	1987
1956	1988
1957	1989
1960	1990
1962	1991
1963	1992
1964	1993
1965	1994
1966	1995
1967	1996
1968	1997
1971	1998
1975	1999
1977	2000
1978	2001
1981	2002

The tropical SST warming mode (Fig. 7) is associated with an increase in 500-mb geopotential height (5–10 m) throughout the tropical atmosphere during the entire summer. The warming of the tropical atmosphere follows from the increase in tropical SST. Irrespective of the possible uncertainty in observed tropospheric warming (e.g., Mears et al. 2003), the trend in tropical geopotential height shown here for the NCEP–NCAR reanalysis has been replicated in GCM simulations forced with observed SST for the period 1950–2000 (Kumar et al. 2004), strongly suggesting that it is real. ENSO also causes a uniform warming of the tropical atmosphere, so the increase in geopotential height due to the tropical SST warming mode is likely weakening

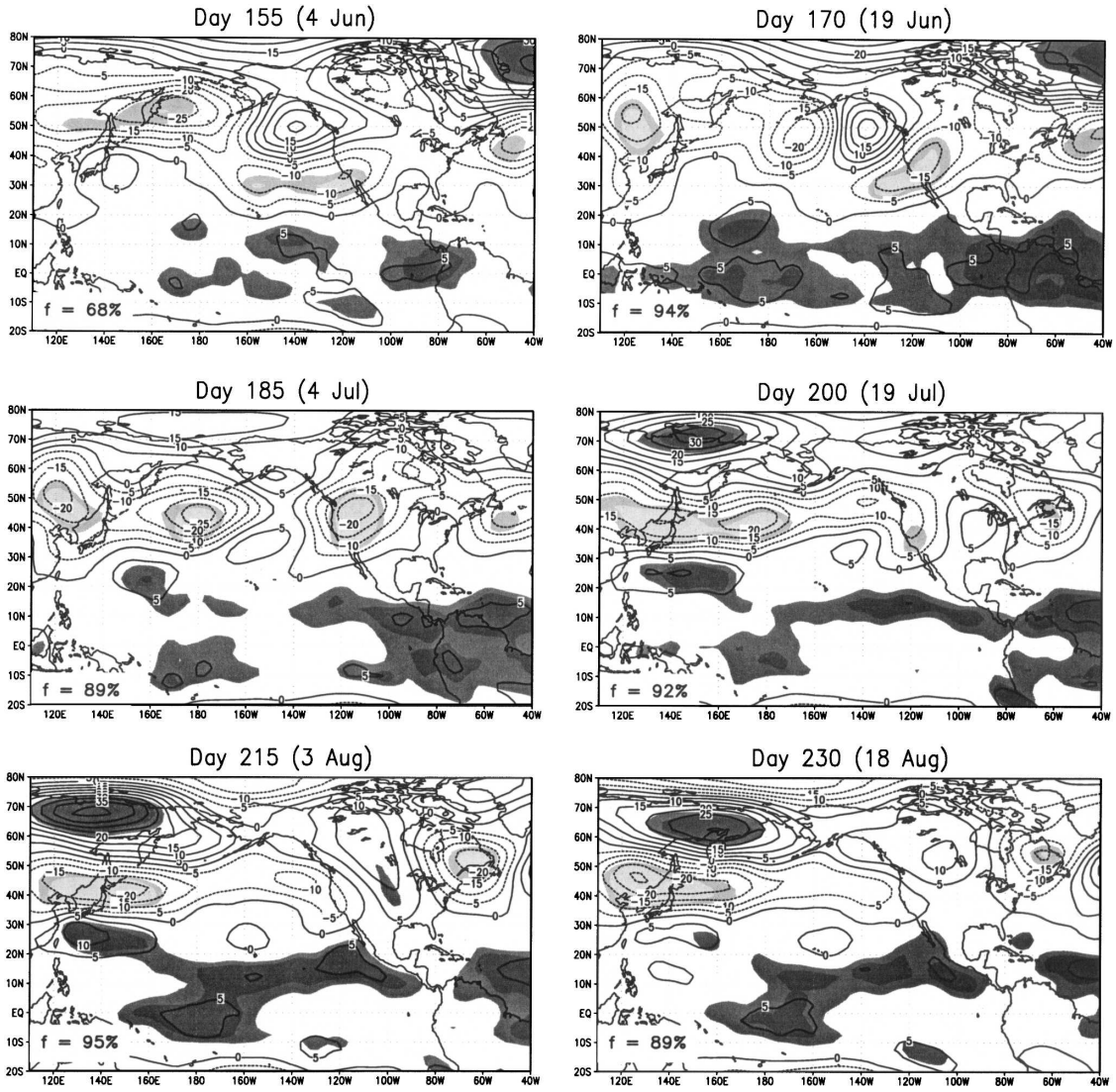

FIG. 5. Time evolution of 30-day average NCEP–NCAR reanalysis 500-mb height anomalies (m) centered on the date through the summer season for Pacific variability mode-1 composites in Table 1. Contour interval is 5 m. Shading indicates local statistical significance at the 90% and 95% levels. Significant positive (negative) anomalies are shaded dark (light). Field significance (f) of shaded areas is indicated on each plot.

the statistical significance of height anomalies in Figs. 5 and 6. Unlike Pacific variability modes, the tropical SST warming mode has no significant relationship to height anomalies in the midlatitudes during the summer.

4. Response of teleconnections in RCM-simulated fields

a. Precipitation

Similar composites were constructed for the RCM 30-day average precipitation differences. The composites based on either Pacific variability mode 1 or 2 were not field significant at the 90% level for most of the summer. A more statistically significant result is achieved if the "Combined Pacific Variability Mode" composites (Table 4) are used as shown in Fig. 8; this makes sense given the teleconnection relationships shown in section 3. The modes associated with interannual and decadal variability constructively interfere with each other to produce the most coherent anomalies, consistent with the behavior for the winter season (Gurshunov and Barnett 1998). The most significant RCM precipitation anomalies in Fig. 8 occur in the central United States (40–60 mm) and in the core monsoon region, defined in Part I as the U.S. Southwest (10–20

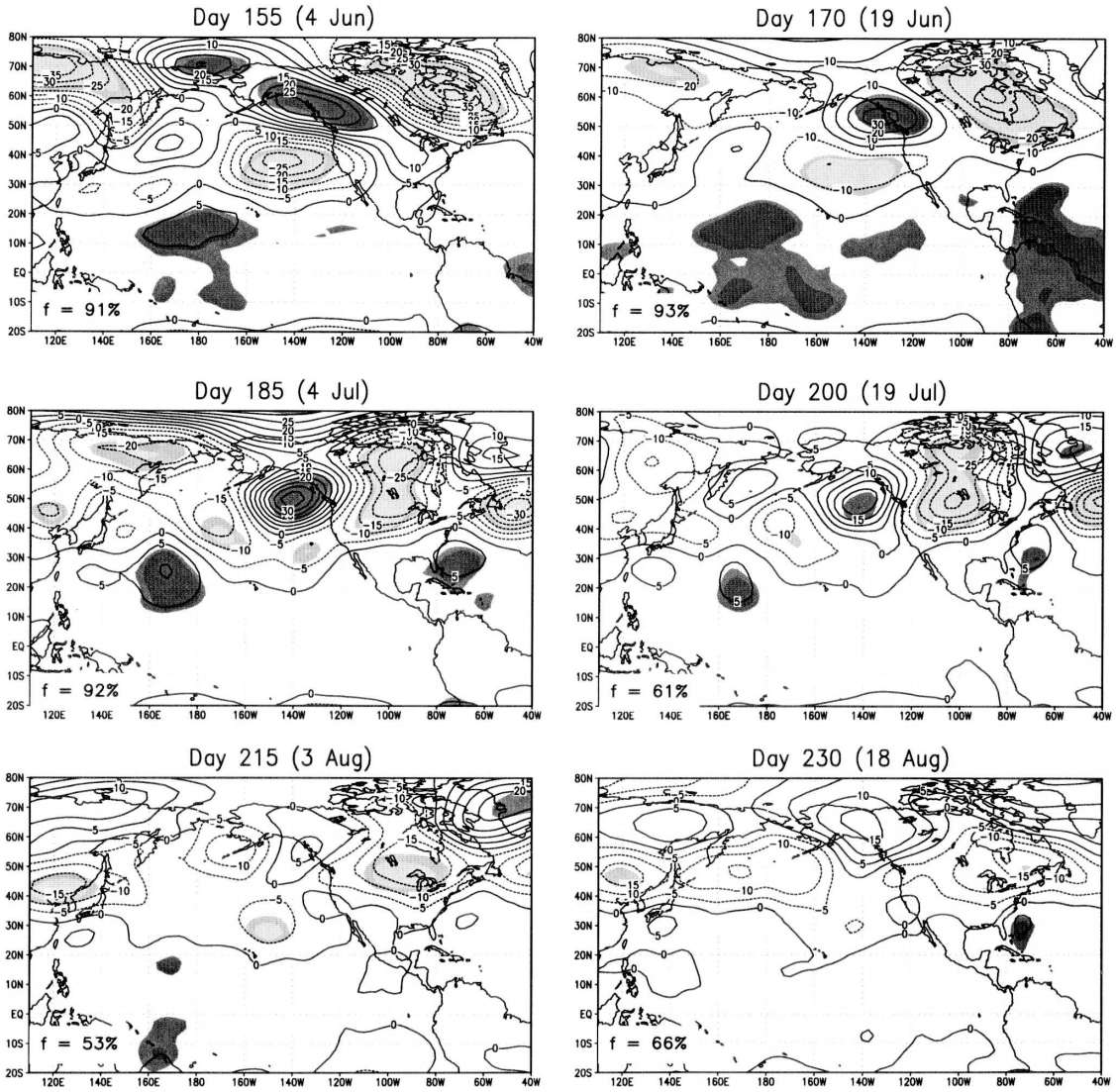

FIG. 6. As in Fig. 5 but for Pacific variability mode-2 composites in Table 2.

mm) and northwest Mexico (30–50 mm). These regions are oppositely related. The timing of the precipitation response is directly linked to the evolution of the teleconnections in Figs. 5 and 6, so the effect of the large-scale forcing as provided by the NCEP GR acts to delay or accelerate the climatological evolution of the NAMS in the RCM. As the teleconnections wane, differences in RCM precipitation become insignificant. Another interesting feature is the reversal in sign of the precipitation anomaly in the U.S. Southwest through late spring into early summer. These results are entirely consistent with previous observational analyses (e.g., Castro et al. 2001; Mo and Paegle 2000).

Figure 9 is similar to Fig. 8, but with the observed Climate Prediction Center (CPC) gauge-derived precipitation (Higgins et al. 1996). Though the precipitation anomalies are not as large, the patterns and levels of significance at the period of maximum teleconnectivity in the contiguous United States are nearly identical to that obtained with the RCM. No significant anomalies exist in western Mexico however, and this is likely because of the poor observational network there, as discussed in Part I. No significant anomalies as in Figs. 8 and 9 appear in the NCEP GR precipitation (not shown). The failure of the NCEP GR to capture the interannual variability in North American summer precipitation makes sense, given its failure to capture the climatological transitions associated with development of the NAMS (as discussed in Part I). In their GCM study focusing on variability in U.S. Southwest rainfall, Ferrara and Yu (2003) ran simulations for the summer season with climatological SSTs and SSTs defined by

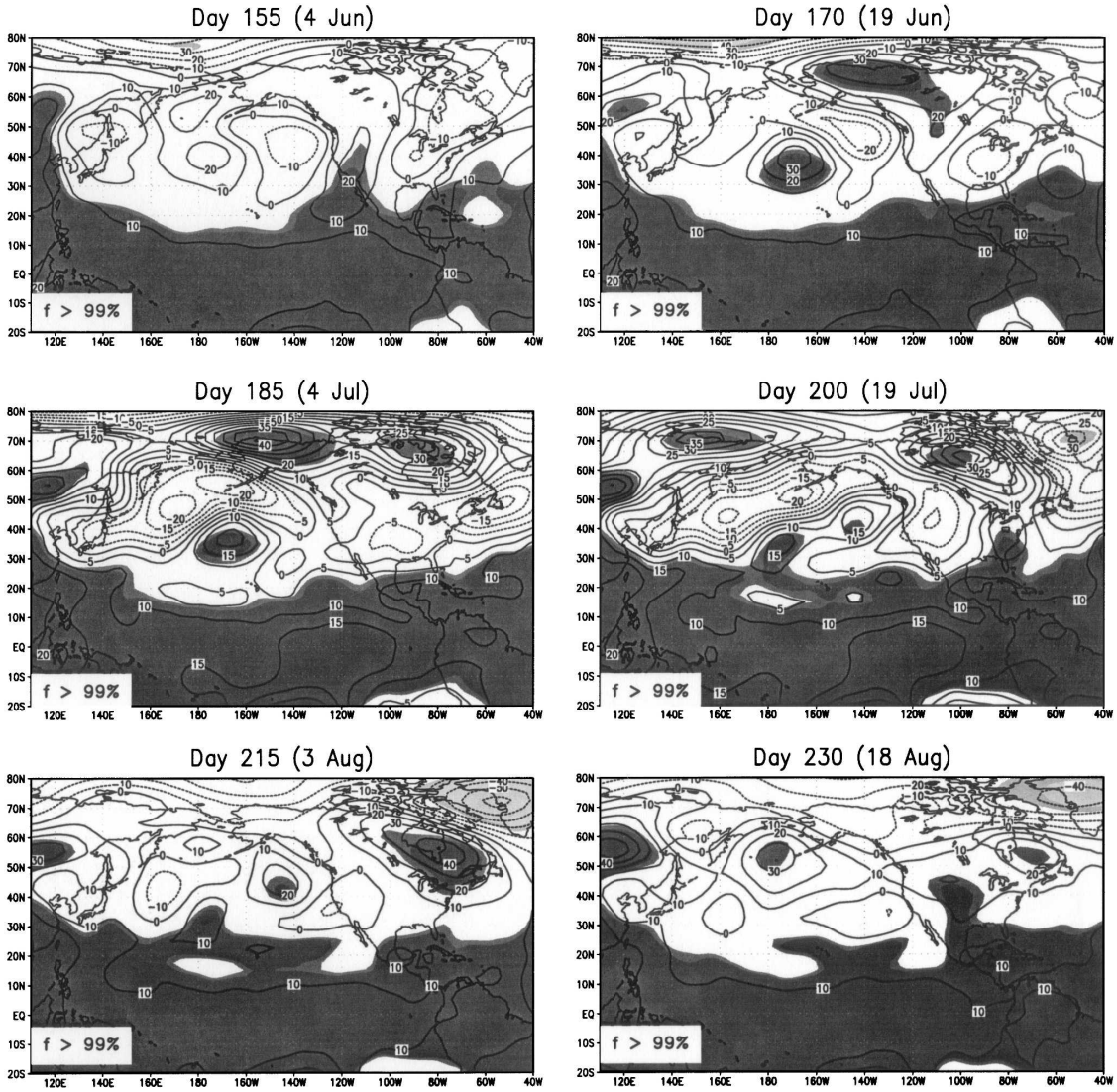

FIG. 7. As in Fig. 5 but for tropical SST warming mode composites in Table 3.

wet and dry monsoon years. Similar to the results using the NCEP–NCAR reanalysis rainfall, they found little difference in precipitation generated by varying SSTs and therefore concluded that the variability between wet and dry years is due to internal atmospheric variability alone. A better representation of the diurnally forced convective rainfall within the RCM, as shown in Part I, and consideration of the time-evolving nature of the summer teleconnections suggests a different conclusion.

The RCM precipitation anomalies associated with the tropical SST warming mode are shown in Fig. 10. The RCM results indicate a general increase in precipitation over the last 20 years in the contiguous United States, particularly east of the continental divide, which does not appear to be time dependent, as in Figs. 8 and 9. Where the changes are statistically significant, the increase in precipitation is on the order of 10%–20%. The increase in rainfall is due to an increase in moisture, presumably from the Tropics, and not changes in the large-scale dynamics (see section 4b). Long-term increases in observed atmospheric moisture and precipitation in the contiguous United States have been documented in the latter half of the twentieth century (e.g., Karl and Knight 1998; Gaffen and Ross 1999; Durre 2006). Stronger relationships between RCM precipitation and the tropical SST warming mode exist in Mexico, even more significant than those associated with the combined Pacific variability mode. The RCM results indicate that precipitation over the last 20 years or so has decreased west of the crest of the Sierra Madre Occidental (SMO) and increased east of the SMO

TABLE 4. As in Table 1 but for the combined Pacific variability mode.

Negative	Positive
1950	1951
1954	1957
1955	1958
1956	1963
1964	1965
1970	1968
1971	1969
1973	1972
1974	1982
1975	1983
1976	1986
1981	1987
1984	1990
1985	1991
1988	1992
1989	1993
1999	1994
2000	1997
2001	
2002	

during the peak of the monsoon there. The decrease is approximately 15% of the RCM climatological rainfall where it is statistically significant. Recent investigations by Cavazos (2006) and Gochis et al. (2006) confirm that there have been long-term decreases in both observed summer rainfall and streamflow in western Mexico. The same analysis for the observed CPC rainfall (not shown) did not produce results that were field significant at the 90% level, and this is most likely due to the poor quality of the long-term precipitation observations in Mexico.

b. Surface temperature and moisture flux

Since section 4a established that the greatest differences in precipitation occur at the period of maximum teleconnectivity (for the combined Pacific variability mode), just the 30-day average about 15 July is shown for the analysis of RCM surface temperature and moisture flux in Fig. 11. The combined Pacific variability mode composite shows a positive relationship with surface temperature in Mexico and adjacent eastern Pacific Ocean and part of the southwest United States and a negative relationship in the northern Great Plains and Rocky Mountains, consistent with reanalysis temperature differences between wet and dry periods in the central United States found by Mo et al. (1997). The temperature anomalies, as is the case for precipitation, mirror the changes in climatology from the monsoon peak minus onset period (see Part I). Temperature anomalies for the tropical SST warming mode show a decrease over the central United States due to the increase in surface moisture. While this decrease is small, it is statistically significant and consistent with station observations (Durre 2006). A more significant increase in surface temperature occurs off the west coast of Baja California, due to the long-term increase in sea surface temperature there as realized by the year-specific SST in the RCM.

The average surface moisture flux anomalies are shown on the bottom panels of Fig. 11. For the combined Pacific variability mode, the most significant differences occur in areas where low-level jets are present. There is a positive association with the Great Plains LLJ, with significant anomalies extending from the Caribbean Sea and Gulf of Mexico into the central United States and Midwest. The largest anomalies occur at the location of the climatological maximum of the Great Plains LLJ in Texas and Oklahoma (10 m s^{-1} g kg^{-1}). There is a negative association with the Baja LLJ in the northern Gulf of California. An increase in the strength of the Baja LLJ would direct more moisture into the Colorado River valley and Arizona (west of the continental divide). A very similar result was recently obtained in an evaluation of the Great Plains and Baja LLJs using a 50-km version of the NCEP Regional Spectral Model for the period 1991–2000 (Mo and Berbery 2004), though in that case the total integrated moisture flux was considered.

A change in the mean strength of both LLJs as related to the combined Pacific SST variability mode should not be surprising given the changes in the atmospheric circulation and surface temperature. The Baja LLJ is fundamentally driven by the temperature gradient across the Gulf of California (e.g., Adams and Comrie 1997) and the mean temperature gradient would be decreased (increased) in years of high (low) phase of the mode. The most likely cause for the variation in the strength of the Great Plains LLJ is the interaction of the large-scale atmospheric flow with the topography (Byerle and Paegle 2003; Mo and Berbery 2004), as this would be directly related to the teleconnection patterns. Stronger (weaker) zonal winds upstream of the Rocky Mountains have a leeside response in the form of a stronger (weaker) Great Plains LLJ. Mechanisms related to the surface forcing and rainfall within the RCM may also be affecting the GP LLJ. Greater latent heating associated with increased rainfall may lead to stronger ascent and southerly flow (Rodwell and Hoskins 2001). Another possibility is that warmer daytime surface temperatures and less surface moisture (a higher Bowen ratio), which occur over New Mexico and the Mexican plateau, coupled with cooler

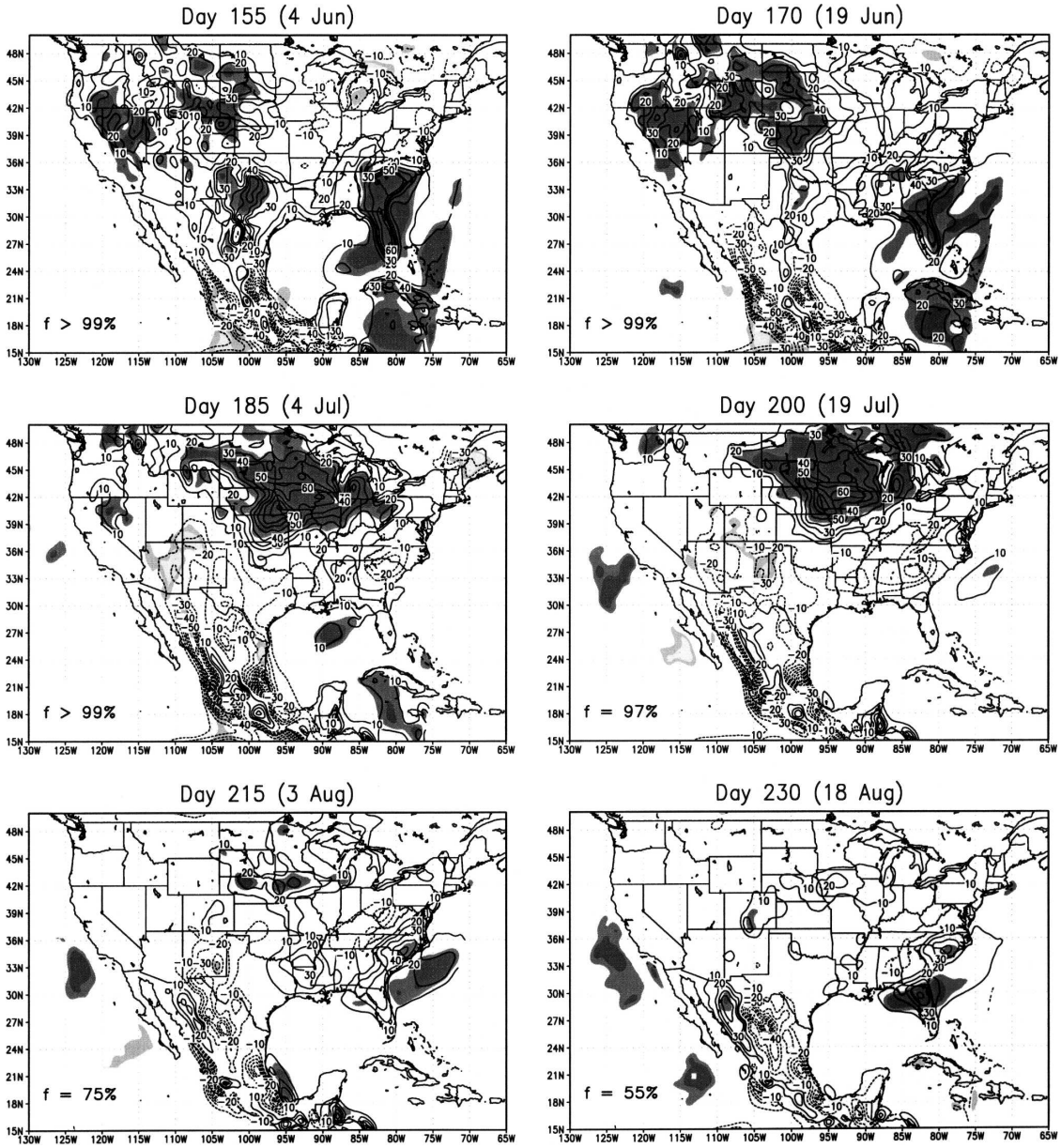

FIG. 8. Time evolution of 30-day average RAMS precipitation anomalies (mm) centered on the date for the combined Pacific variability mode composites in Table 4. Contour interval is 10 mm. Shading indicates local statistical significance at the 90% and 95% levels. Significant positive (negative) areas are shaded dark (light). Field significance (f) of shaded areas is indicated on each plot.

and more moist conditions to the east would intensify the terrain-induced pressure gradient and, hence, the LLJ (Mo et al. 1997). This agrees with the idealized modeling study of the Great Plains LLJ by McNider and Pielke (1981). McNider and Pielke also note that cumulus formation to the east of the dryline in the Great Plains would enhance the baroclinicity.

The changes in the Great Plains LLJ in relation to the combined Pacific variability mode are very close to what has been observed in comparing dry and wet periods in the central United States using NCEP–NCAR reanalysis data (e.g., Mo et al. 1997). Where RAMS adds more value is in the representation of the Baja LLJ in the Gulf of California. The area in the northern Gulf of California where significant anomalies are found contains only one or two grid points in the NCEP–NCAR reanalysis. As with other fields, the interannual differences in the LLJs associated with the

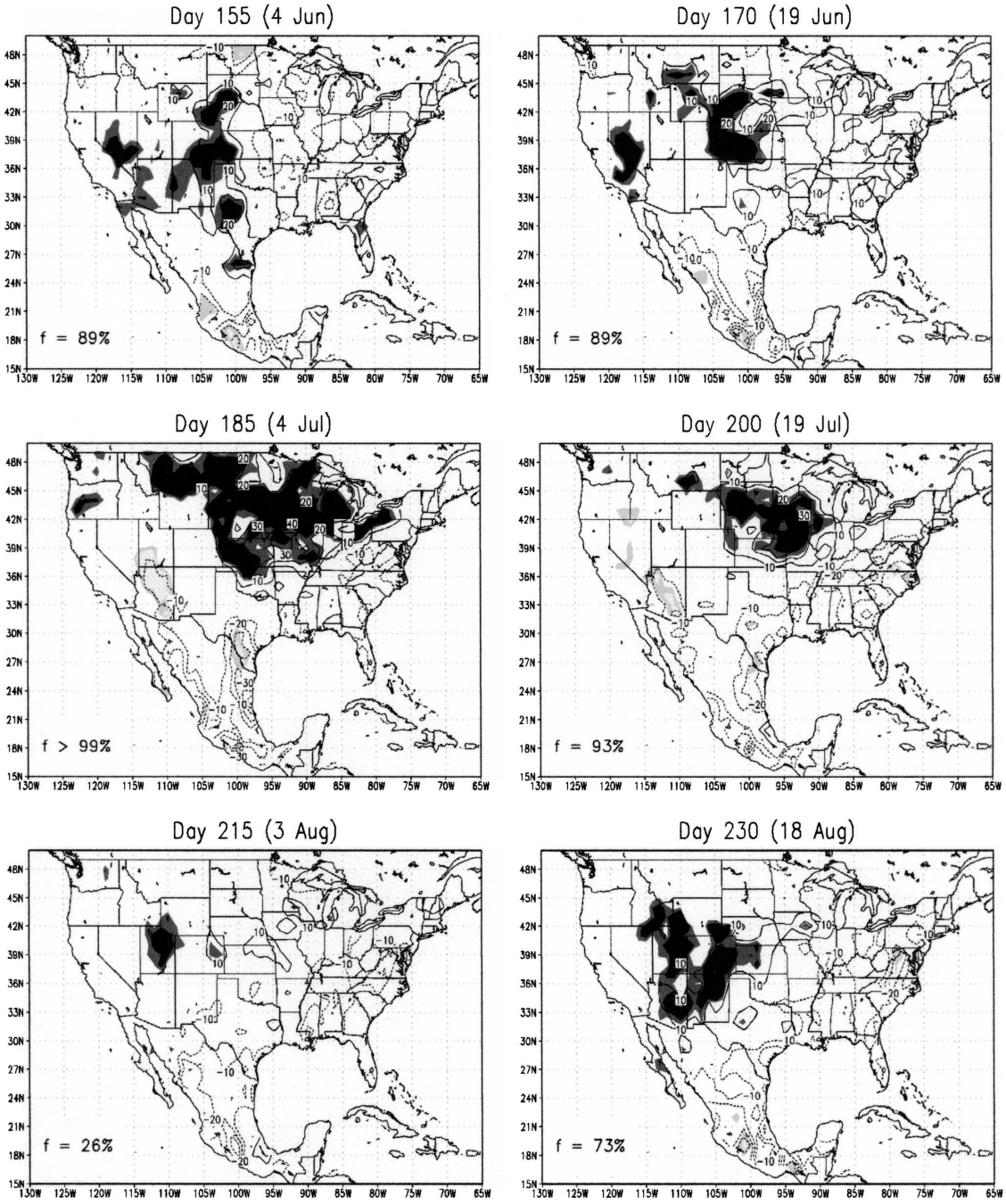

FIG. 9. As in Fig. 8 but for observed gauge-derived CPC precipitation.

combined Pacific variability mode mirror the changes that occur climatologically between the monsoon peak minus premonsoon period. They also mirror the change observed during a modeled Gulf surge event in RAMS, with increased winds in the Gulf of California and a more easterly component of the Great Plains LLJ (Saleeby and Cotton 2004). RAMS tended to underestimate the strength of the Baja LLJ and associated gulf surges in these RCM simulations (see Part I), so it is likely that the actual surface moisture flux anomalies in this area associated with the combined Pacific variability mode are greater in magnitude and extend through most of the length of the Gulf of California. Nonetheless, the difference in moisture transport is sufficient to cause a significant change in U.S. Southwest rainfall (Fig. 8).

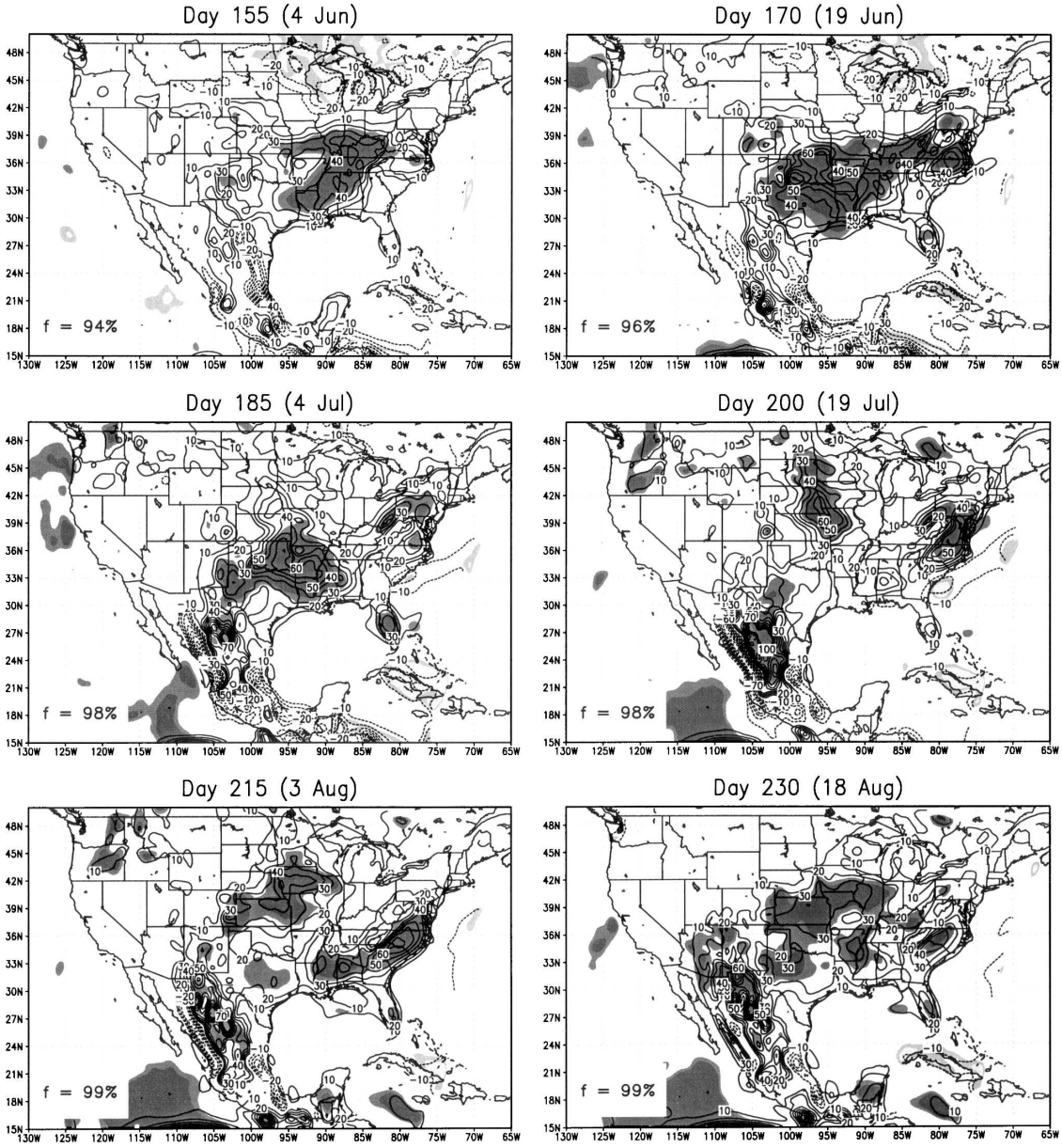

FIG. 10. As in Fig. 8 but for RAMS precipitation anomalies for the tropical SST warming mode composite in Table 3.

The changes in surface moisture flux associated with the tropical SST warming mode are shown in the lower right of Fig. 11. Unlike the combined Pacific variability mode, the significant changes in moisture flux over the contiguous United States are not due to changes in the LLJs. An analysis of the RCM winds and moisture considered separately (not shown) confirmed that these changes reflect the general increase in summertime moisture over the latter part of the record. The area in the domain where there is the largest decrease in moisture flux is off the west coast of Mexico south of Baja California (about 5% of the climatological mean). This is caused by the local decrease in the sea surface temperature gradient in this region, as indicated by the change in surface temperature. The long-term increase in sea surface temperature in the subtropical eastern Pacific off the west coast of Mexico (0.4 to 0.6 K) since the early 1980s is thus the cause of the significant decrease in RCM precipitation in western Mexico. Because the RCM incorporates year-specific SSTs, as mentioned, this result is due to a local change in the surface boundary within the RCM domain and not large-scale forcing by the GR. This also helps to establish a physical basis for the statistical relationship be-

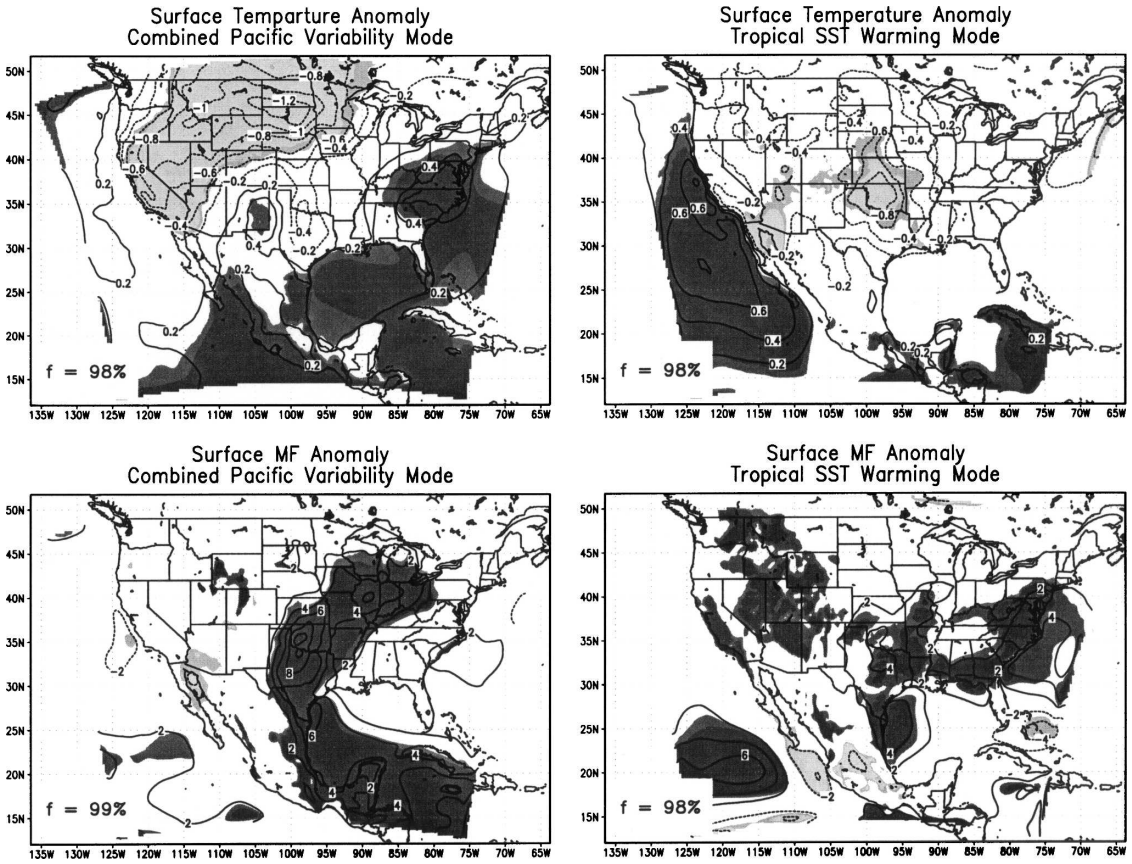

FIG. 11. The 30-day average surface temperature (K) and moisture flux (g kg^{-1} m s^{-1}) anomalies for combined Pacific variability mode composites in Table 4 and tropical SST warming mode composites in Table 3 at the period of maximum teleconnectivity (see text for details). Contour interval for temperature is 0.2 K and contour interval for moisture flux is 2 g kg^{-1} m s^{-1}. Shading indicates local statistical significance at the 90% and 95% levels. Significant positive (negative) anomalies are shaded dark (light). Field significance (f) of shaded areas is indicated on each plot.

tween NAMS precipitation and eastern tropical Pacific SSTs, as noted, for example, by Carleton et al. (1990).

c. *Time-varying modes of integrated moisture flux convergence*

In Part I, a method to spectrally decompose integrated moisture flux convergence (MFC) into its dominant time-varying modes using a spectral analysis technique was presented. MFC is considered because it is a proxy for convective rainfall. The weighted spectral power of MFC as the fraction of spectral power above climatological red noise in a frequency band was considered. Three distinct frequency bands were specified: a synoptic mode (4–15 days), a subsynoptic mode (1.5–3 days), and a diurnal mode. Here the interest is in the difference in spectral power, computed in the same way as composite anomalies shown in preceding parts of this section. This quantity is multiplied by the weighting factor (W), so only areas where the climatological spectrum exceeds red noise are emphasized. This is referred to as the fractional difference in weighted spectral power.

As in Fig. 11, only a date for the period of maximum teleconnectivity for the Pacific SST variability mode in July is shown in Fig. 12 for the combined Pacific variability mode and the tropical SST warming mode. The specific July date is chosen that approximately shows the maximum fractional difference in weighted spectral power. For the diurnal and synoptic bands this date is 15 July and for the subsynoptic band it is 4 July. Similar patterns of differences were observed from early to mid July. The statistical significance of the fractional difference in weighted spectral power is not assessed for the composites. This analysis is only intended to show that the spatial patterns of difference in the spectral bands correspond well with the statistically significant differences in precipitation already described.

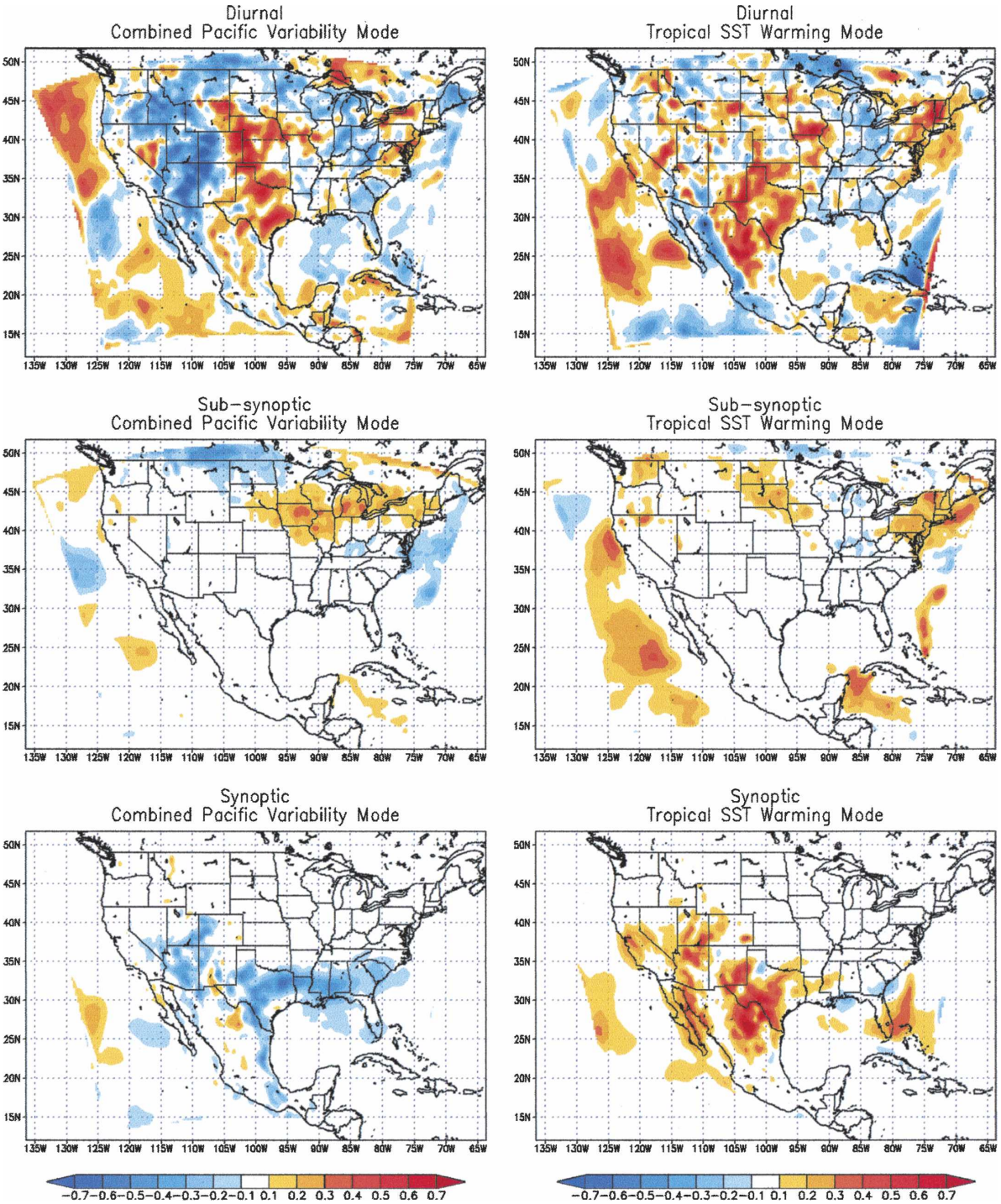

FIG. 12. Fractional difference in weighted spectral power of MFC for combined Pacific variability mode composites in Table 4 and tropical SST warming mode composites in Table 3 at period of maximum teleconnectivity (see text for details). Shown are the diurnal (1 day), subsynoptic (1.5–3 day), and synoptic (4–15 day) bands. Shading indicated by color bars.

The combined Pacific variability mode is considered first. The diurnal cycle differences are the most important because this is where the RCM adds the most value in representation of summer rainfall (see Part I). The diurnal cycle is the dominant mechanism for rainfall generation in the U.S. Southwest and Great Plains, and the largest differences occur between these regions. Its intensity can vary up to 70% in years with differing

phases of the combined Pacific variability mode. The demarcation between these regions with opposite signals is quite sharp and is roughly the continental divide. Given the changes already seen in the LLJs, this suggests that the continental divide provides a physical barrier separating the moisture coming from each low-level source. Thus, there can be large differences in the interannual variability of diurnal convection for distances smaller than the typical grid spacing of a GCM or GR (100s of km). The most striking example is in Colorado. The Eastern Plains and Western Slope regions of the state have strongly opposite signals. A higher nocturnal peak in rainfall in the high phase of the combined Pacific variability mode would correspond with more intense eastward propagating mesoscale convective complexes in the Great Plains, in agreement with Hu (2003).

While the lower frequency modes of MFC have less weighted spectral power, their relationship to the combined Pacific variability mode is nonetheless just as striking and also consistent with the teleconnections. The subsynoptic component of MFC reflects convection occurring beyond the diurnal time scale from fast-moving synoptic weather systems or propagating mesoscale convective systems (MCSs) around the northeastern periphery of the monsoon ridge. Since these MCSs typically originate as diurnal convection over the Rocky Mountains, the variation in the MCS signal in the upper Midwest is consistent with the diurnal variation to the west. The weighted spectral power in the subsynoptic changes on the order of 20%–30% in Iowa, northern Illinois, Wisconsin, and Michigan. This area is approximately the location of largest rainfall anomalies in the contiguous United States in Fig. 8.

The synoptic mode of MFC is related to the passage of large-scale, westward propagating disturbances (i.e., tropical easterly waves, inverted troughs, or tropical cyclones) around the southern periphery of the monsoon ridge. These cause periodic enhancement of the diurnal convection, which may propagate westward off the terrain and organize into MCSs in the core monsoon region. As with its climatology, this mode shows that the largest changes associated with the combined Pacific variability mode occur at lower elevation and it again varies as the diurnal cycle in the core monsoon region. There are two possible reasons for the change in spectral power in this mode. First, there may be a change in the strength of westward propagating disturbances, which trigger the convective bursts. Second, the strength of the easterly disturbances does not change but, because of the change in mean moisture transport from the Gulf of California, the disturbances trigger larger and more widespread convective outbursts in years with a low phase of the Pacific SST variability mode. The southeast United States is also noteworthy. In Texas, for example, variability in synoptic MFC behaves opposite to that of the diurnal mode, implying that the diurnal cycle and synoptic variability of rainfall are not linked there.

The changes in the variability of MFC associated with the tropical SST warming mode, shown on the right-hand side of Fig. 12, match the precipitation anomalies in Fig. 10. In this case, the largest and most coherent changes in the diurnal cycle occur in Mexico, not the contiguous United States. The clear dividing line between the regions with opposite signals is the continental divide along the crest of the SMO. To the west of the divide, the intensity of the diurnal cycle has decreased over the past 20 years by 30%–50%. The lower frequency modes show increases, owing to the general increase in moisture over the contiguous United States. The long-term increase in synoptic MFC over the Southwest may act to enhance rainfall during the latter part of the monsoon in August once the effect of the summer teleconnections diminish.

5. Discussion

A necessary prelude to the analysis of RCM results in this study was a characterization of boreal summer global SST and the relationship of its dominant modes to variability in the large-scale atmospheric circulation. An extension of the SST REOF analysis of Schubert et al. (2002) produced three dominant modes. Two of these modes correspond to known and statistically significant variability in Pacific SST at the interannual and interdecadal time scales. It is these naturally occurring modes that govern the position of the monsoon ridge over the continent at monsoon onset in late June and early July, as originally described in Castro et al. (2001). This period defines the period of maximum teleconnectivity. These modes constructively interfere with each other, so the most coherent anomaly patterns occur when both are of the same phase. Similar teleconnections are generated in idealized modeling and GCM studies, including those of Schubert et al. (2002) as detailed in Castro (2005). Consideration of the time-evolving nature of these teleconnections is essential to understanding summer climate variability in North America.

The remaining SST mode reflected a global increase in tropical SST, particularly after about 1980 or so. Was it fair to consider this mode as a distinct entity from the other two, even though it may not be clearly separated

from decadal variability in the 1950–2000 record? We assert the answer to this question is yes for several reasons: 1) the cause of this warming has not been conclusively ascertained; 2) it is not associated with a time-evolving teleconnection in the midlatitudes, as are the other modes; and 3) most important, the effect on North American summer climate due to the change in eastern tropical Pacific SST is very distinct and statistically significant, particularly in Mexico.

In Part I, we demonstrated the value added by RCM dynamical downscaling in a Type-2 mode (Castro et al. 2005) to create the summer climatology of North America. The greatest differences between RCM and NCEP–NCAR reanalysis climatological rainfall occur in areas where the diurnal cycle of convection is the dominant rainfall mechanism, specifically the core monsoon region and the central United States. These are exactly the same areas that have the most statistically significant relationships between summer rainfall and Pacific SST variability. The changes in the strength of the diurnal cycle of MFC (Fig. 12, upper left) associated with the combined Pacific variability mode dramatically show how the surface forcing interacts with the large-scale atmospheric dynamics (provided to the RCM) to organize the terrain-induced convective rainfall. Because a GCM or GR cannot capture this essential detail, their conclusions regarding summer climate variability in North America, and its potential predictability, may be incorrect. A specific example was provided in section 4 to illustrate this point.

In considering the effect of the recent tropical SST warming, the RCM especially added value to understanding how the change in the SST gradient in the eastern tropical Pacific off the Mexican coast may be impacting Mexican summer rainfall. In the RCM, a decrease in the SST gradient causes a decrease in the transport of atmospheric moisture from the eastern Pacific into western Mexico. Subsequently, a decrease in diurnally generated convective rainfall occurs west of the crest of the SMO. This effect is realized by the RCM representation of the surface boundary, and not by the influence of the larger-scale forcing by the GR. Because of the poor quality of long-term precipitation observations in Mexico this trend is not resolved in the CPC observations, but it has been confirmed in other investigations. The physical explanation the RCM results offer to understanding long-term trends in Mexican rainfall may be the most important result of the present investigation. Given the potential societal ramifications in terms of water supply and agriculture for this region, further investigation of this issue is warranted.

The results presented herein are only a statistical analysis of RCM simulations in a seasonal weather simulation mode, or Type-2 dynamical downscaling, in which an atmospheric reanalysis is used to specify the forcing to the RCM (Castro et al. 2005). To establish the physical link to remote SST forcing, seasonal weather prediction (Type-3 dynamical downscaling) is necessary, in which the RCM forcing is provided by a GCM with specified SST. We did perform additional RCM simulations of this type, dynamically downscaling the aforementioned NSIPP GCM data of Schubert et al. (2002). A complete description of these experiments and results is given in Castro (2005), and here we briefly summarize the two main conclusions. First, the driving GCM should be able to produce a reasonable summer climatology, which we would define as being on par with a global atmospheric reanalysis. Second, the GCM must be able to reproduce the time-evolving teleconnections in Figs. 5 and 6 when forced with idealized SST distributions corresponding to the modes of variability in the Pacific. For the NSIPP GCM simulations, the "best" teleconnection response occurred for the positive phase of Pacific variability mode 2, as shown in Fig. 13. A comparison of the dynamical downscaling results of the NCEP–RAMS and NSIPP–RAMS for this mode is shown in Fig. 14, corresponding to the analyses in the previous section (but only the positive phase of the mode shown in this case). Both sets of RCM simulation show an increase in precipitation in the central United States and a decrease in the core monsoon region; cooler surface temperatures in the northern Rockies and northern Great Plains and warmer surface temperatures in Mexico; a strengthened Great Plains LLJ; and a strong demarcation at the continental divide between areas with a stronger and weaker diurnal cycle of convection.

Finally, we would be quite remiss if we did not mention the potential impact of the land surface on North American summer climate variability. This includes antecedent snow cover (Gutzler and Preston 1997; Gutzler 2000; Lo and Clark 2002; Zhu et al. 2005), soil moisture (e.g., Wang and Kumar 1998; Hong and Pan 2000; Pal and Eltahir 2001; Small 2001; Hong and Kalnay 2002; Kanamitsu and Mo 2003; Pal and Eltahir 2003), and vegetation (e.g., Pielke 2001; Lu and Shuttleworth 2002; Matsui et al. 2005; Adegoke et al. 2006). These effects have been evaluated in both observational and regional and global modeling frameworks in the aforementioned studies. Our future work with the RAMS model will use the present set of RCM simulations as a baseline to evaluate the influence of the land surface in different SST regimes.

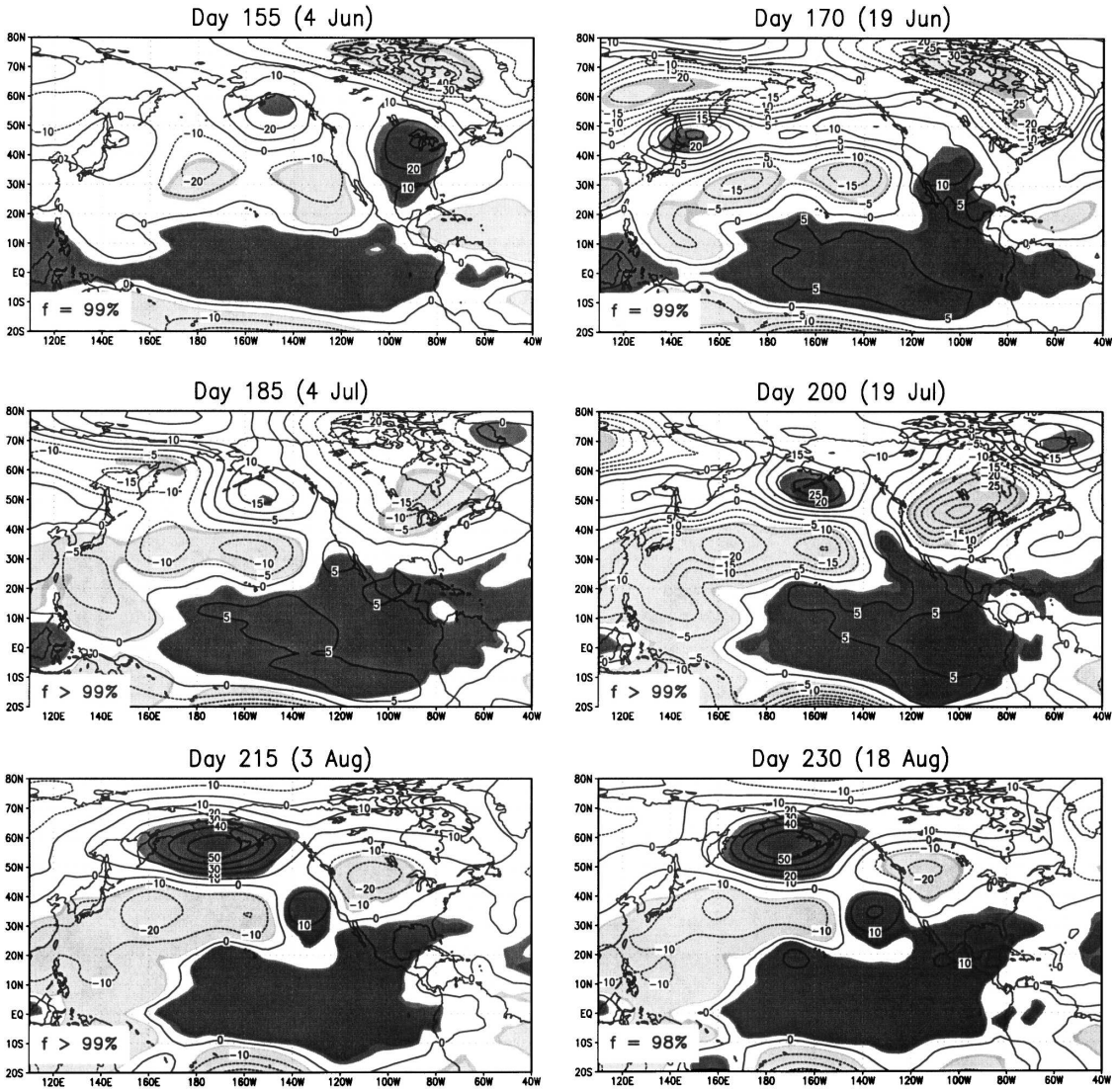

FIG. 13. Time evolution of 30-day average NSIPP GCM 500-mb height anomalies (m) centered on the date for Pacific variability mode-2 positive ensemble, from simulations originally described in Schubert et al. (2002). Contour intervals and statistical significance as in Fig. 5.

6. Summary

Summer dynamical downscaling simulations over the contiguous United States and Mexico with RAMS from Part I were evaluated with respect to the three dominant modes of global SST. Two of these modes are associated with naturally occurring interannual and interdecadal variability in the Pacific. The remaining mode corresponds to the recent warming of tropical sea surface temperatures. Consistent with prior work, time-evolving teleconnections associated with Pacific SSTs delay or accelerate NAMS evolution. At the period of maximum teleconnectivity in late June and early July, there is an opposite relationship between precipitation in the core monsoon region and the central United States. Use of the RCM is essential to capture this variability because of its representation of the diurnal cycle of convective rainfall. The RCM also added value in representing observed long-term changes in Mexican rainfall and suggests that these are likely due to the recent increase in eastern Pacific SST within the model domain. An additional series of RAMS seasonal weather prediction mode simulations was also briefly discussed. These dynamically downscaled data from a GCM forced with the Pacific modes to establish the physical linkage to remote SST forcing. In order for

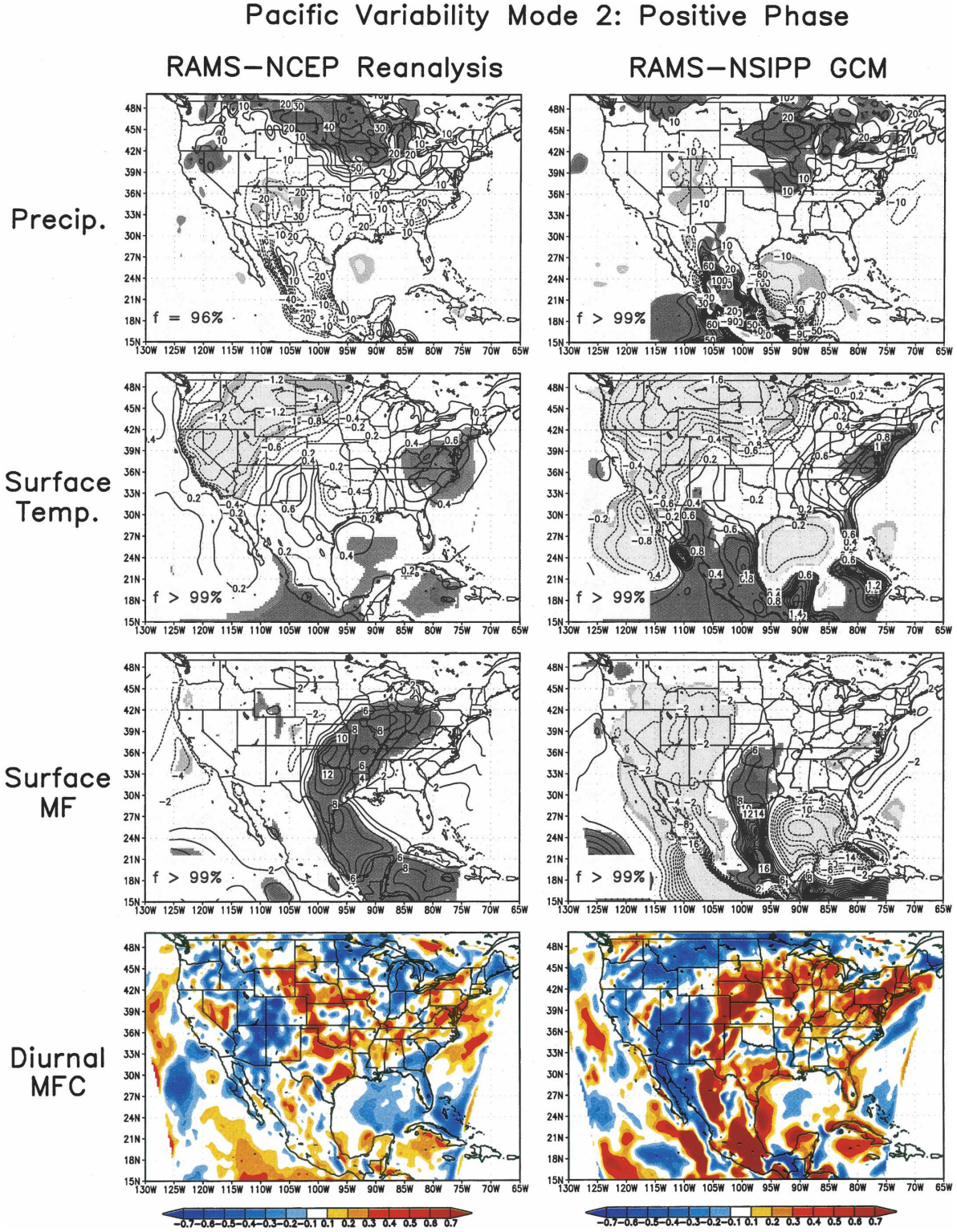

FIG. 14. Comparison of Pacific variability mode-2 positive phase at the period of maximum teleconnectivity for RAMS–NCEP composite (30-day average centered on 15 Jul) and RAMS–NSIPP ensembles (30-day average centered on 20 Jul). RAMS–NCEP composite years are defined in Table 1. Anomalies of precipitation, surface temperature, surface moisture flux (MF), and diurnal MFC are considered the same as in previous figures in section 4. RAMS–NSIPP simulations are described in Castro (2005).

RCMs to be successful in a seasonal weather prediction mode for the summer season it is required that the GCM have a climatology comparable to a global atmospheric reanalysis and provide a reasonable representation of the time-evolving teleconnections.

Acknowledgments. This research was funded by NOAA Grant NA17RJ1228 Amendment 6 and NASA Grant NGT5-30344. The authors thank Michael Kistler for preparing the NSIPP GCM data. Drs. David W. J. Thompson and William R. Cotton provided comments that improved the original manuscript. Two anonymous reviewers and *Journal of Climate* editor Dr. David Straus also provided very helpful comments during the revision process.

APPENDIX

Summary of the MTM–SVD Method

The following is a brief summary of the MTM–SVD method used for the SST analysis in section 2 and follows from Mann and Park (1994, 1996) and Rajagopalan et al. (1998). The specific analysis routines are freely available online from M. Mann at the Pennsylvania State University, and are the same as used in Rajagopalan et al. (1998).

For the given time series y (SST in this case), a set of K orthogonal data tapers and K associated tapered Fourier transforms (eigenspectra) is determined at each frequency f by

$$Y_k^{(m)}(f) = \sum_{t=1}^{N} w_t^{(k)} y_n e^{i2\pi ft\Delta t}, \tag{A1}$$

where Δt is the sampling interval (1 month), $\{w_t^{(k)}\}_{t=1}^{N}$ is the kth member in an orthogonal series of (Slepian) data tapers, $k = 1, \ldots, K$; $m = 1, \ldots, M$ are the number of grid points with data; and N is the length of the time series. Only the first $k = 2p - 1$ data tapers are usefully resistant to spectral leakage. A choice of $p = 2$ and $k = 3$ tapers is used, as it provides good frequency resolution and sufficient spectral degrees of freedom. At each frequency point, the $M \times K$ matrix is

$$\mathbf{A}(f) = \begin{bmatrix} w_1 Y_1^{(1)} & w_1 Y_2^{(1)} & & w_1 Y_K^{(1)} \\ w_2 Y_1^{(2)} & w_2 Y_2^{(2)} & & w_2 Y_K^{(2)} \\ & & \ddots & \\ w_M Y_1^{(M)} & w_M Y_2^{(M)} & & w_M Y_K^{(M)} \end{bmatrix}, \tag{A2}$$

where w represent gridpoint-specific weightings for latitude. A complex SVD is performed on the above matrix:

$$\mathbf{A}(f) = \sum_{k=1}^{K} \lambda_k(f)\mathbf{u}_k(f) \times \mathbf{v}_k^*(f), \tag{A3}$$

where the asterisk denotes complex conjugate: λ_k describes the relative fraction of total variance explained by the kth mode, its associated left eigenvector $\mathbf{u}_k^*$ represents the spatial EOFs, and $\mathbf{v}_k$ describes the spectral EOFs.

Within the scale of resolvable frequencies, the fractional variance explained by the kth mode, or local fractional variance (LFV), is

$$\lambda_k^2 \Big/ \sum_{j=k}^{K} \lambda_j^2.$$

Significance of peaks in the LFV spectrum is obtained through a bootstrapping procedure in which the noise at each gridpoint time series is assumed locally white over the bandwidth of eigentapers. In the bootstrap procedure, the spatial fields are randomly resampled 1000 times. The reconstruction of the spatiotemporal signal corresponding to the statistically significant frequencies in the LFV spectrum, as shown in Fig. 1, is described in appendix B of Mann and Park (1994).

REFERENCES

Adams, D. K., and A. C. Comrie, 1997: The North American monsoon. *Bull. Amer. Meteor. Soc.,* **78,** 2197–2213.

Adegoke, J. O., R. A. Pielke Sr., and A. M. Carleton, 2006: Observational and modeling studies of the impacts of agriculture-related land use change on climate in the central U.S. *Agric. Forest Meteor.,* in press.

Alexander, M. A., I. Bladé, M. Newman, J. R. Lanzante, N. C. Lau, and J. D. Scott, 2002: The atmospheric bridge: The influence of ENSO teleconnections on air–sea interaction over the global oceans. *J. Climate,* **15,** 2205–2231.

Barnett, T. P., D. W. Pierce, and R. Schnur, 2001: Detection of anthropogenic climate change in the world's oceans. *Science,* **292,** 270–274.

——, and Coauthors, 2005: Penetration of human-induced warming into the world's oceans. *Science,* **309,** 284–287.

Byerle, L., and J. Paegle, 2003: Modulation of the Great Plains low level jet and moisture transports by orography and large scale circulation. *J. Geophys. Res.,* **108,** 8611, doi:10.1029/2002JD003005.

Carleton, A. M., D. A. Carpenter, and P. J. Weser, 1990: Mechanisms of interannual variability of the southwest United States summer rainfall maximum. *J. Climate,* **3,** 999–1015.

Castro, C. L., 2005: Investigation of the summer climate of North America: A regional atmospheric modeling study. Ph.D. dissertation, Colorado State University, 210 pp.

——, T. B. McKee, and R. A. Pielke Sr., 2001: The relationship of the North American monsoon to tropical and North Pacific

sea surface temperatures as revealed by observational analyses. *J. Climate,* **14,** 4449–4473.

——, R. A. Pielke Sr., and G. Leoncini, 2005: Dynamical downscaling: Assessment of value restored and added using the Regional Atmospheric Modeling System (RAMS). *J. Geophys. Res.,* **110,** D05108, doi:10.1029/2004JD004721.

——, ——, and J. O. Adegoke, 2007: Investigation of the summer climate of the contiguous United States and Mexico using the Regional Atmospheric Modeling System (RAMS). Part I: Model climatology (1950–2002). *J. Climate,* **20,** 89–110.

Cavazos, T., 2006: Extreme Climate indices in the monsoon region: 1950–2004. *Proc. Monsoon Region Climate Applications: A Binational Workshop*. Guaymas, Sonora, Mexico, Instituto Technológico de Sonora (ITSON).

——, A. C. Comrie, and D. M. Liverman, 2002: Intraseasonal variability associated with wet monsoons in southeast Arizona. *J. Climate,* **15,** 2477–2490.

Chiang, J. C. H., and D. J. Vimont, 2004: Analogous Pacific and Atlantic meridional modes of tropical atmosphere–ocean variability. *J. Climate,* **17,** 4143–4158.

Deser, C., M. A. Alexander, and M. S. Timlin, 2003: Understanding the persistence of sea surface temperature anomalies in midlatitudes. *J. Climate,* **16,** 57–72.

Durre, I., 2006: Explaining U.S. precipitation and temperature trends. *Proc. 31st Annual Climate Diagnostics and Prediction Workshop,* Boulder, Colorado, NOAA CDC and CPC of NCEP.

Englehart, P. J., and A. V. Douglas, 2002: On some characteristic variations in warm season precipitation over the central United States (1910–2000). *J. Geophys. Res.,* **107,** 4286, doi:10.1029/2001JD000972.

——, and ——, 2003: Assessing warm season drought episodes in the central United States. *J. Climate,* **16,** 1831–1842.

Ferrara, J. D., and J.-Y. Yu, 2003: Interannual variations in the southwest U.S. monsoon and sea surface temperature anomalies: A general circulation model study. *J. Climate,* **16,** 1703–1720.

Gaffen, D. J., and R. J. Ross, 1999: Climatology and trends of U.S. surface humidity and temperature. *J. Climate,* **12,** 811–828.

Gochis, D. J., L. Brito-Castillo, and W. J. Shuttleworth, 2006: Correlations between sea surface temperatures and warm season streamflow in northwest Mexico. *Int. J. Climatol.,* in press.

Gurshunov, A., and T. B. Barnett, 1998: Interdecadal modulation of ENSO teleconnections. *Bull. Amer. Meteor. Soc.,* **79,** 2715–2725.

Gutzler, D. S., 2000: Covariability of spring snowpack and summer rainfall across the southwest United States. *J. Climate,* **13,** 4018–4027.

——, and J. W. Preston, 1997: Evidence for a relationship between spring snow cover in North America and rainfall in New Mexico. *Geophys. Res. Lett.,* **24,** 2207–2210.

Hansen, J., and Coauthors, 2005: Earth's energy imbalance: Confirmation and implications. *Science,* **308,** 1431–1435.

Higgins, R. W., and W. Shi, 2001: Intercomparison of the principal modes of interannual variability of the North American monsoon system. *J. Climate,* **14,** 403–417.

——, J. E. Janowiak, and Y. Yao, 1996: *A Gridded Hourly Precipitation Data Base for the United States (1963–1993)*. NCEP Climate Prediction Center Atlas 1, 47 pp.

——, Y. Chen, and A. V. Douglas, 1999: Interannual variability of the North American warm season precipitation regime. *J. Climate,* **12,** 653–680.

Hoerling, M., and A. Kumar, 2003: The perfect ocean for drought. *Science,* **299,** 691–694.

Hong, S. Y., and H. L. Pan, 2000: Impact of soil moisture anomalies on seasonal summer circulation over North America in a regional climate model. *J. Geophys. Res.,* **105** (D24), 29 625–29 634.

——, and E. Kalnay, 2002: The 1998 Oklahoma–Texas drought: Mechanistic experiments with NCEP global and regional models. *J. Climate,* **15,** 2469–2480.

Hu, Q., 2003: A multidecadal variation in summer season diurnal rainfall in the central United States. *J. Climate,* **16,** 174–178.

——, and S. Feng, 2001: Variations of teleconnection of ENSO and interannual variation in summer rainfall in the central United States. *J. Climate,* **14,** 2469–2480.

——, and ——, 2002: Interannual variations in the North American summer monsoon region: 1900–98. *J. Climate,* **15,** 1189–1203.

Kalnay, E., and Coauthors, 1996: The NCEP/NCAR 40-Year Reanalysis Project. *Bull. Amer. Meteor. Soc.,* **77,** 437–471.

Kanamitsu, M., and K. C. Mo, 2003: Dynamical effect of land surface processes on summer precipitation over the southwestern United States. *J. Climate,* **16,** 496–503.

Kaplan, A., M. Cane, Y. Kushnir, A. Clement, M. Blumenthal, and B. Rajagopalan, 1998: Analysis of global sea surface temperatures 1856–1991. *J. Geophys. Res.,* **103,** 18 567–18 589.

Karl, T. R., and R. W. Knight, 1998: Secular trends of precipitation amount, frequency, and intensity in the United States. *Bull. Amer. Meteor. Soc.,* **79,** 231–241.

Karspeck, A. R., R. Seager, and M. A. Cane, 2004: Predictability of tropical decadal variability in an intermediate model. *J. Climate,* **17,** 2842–2850.

Kumar, A., F. Yang, L. Goddard, and S. Schubert, 2004: Differing trends in the tropical surface temperature and precipitation over land and oceans. *J. Climate,* **17,** 653–664.

Lau, K. M., and L. Peng, 1992: Dynamics of atmospheric teleconnections during the northern summer. *J. Climate,* **5,** 140–158.

Levitus, S., J. I. Antonov, T. P. Boyer, and C. Stephens, 2000: Warming of the world ocean. *Science,* **287,** 2225–2229.

Livezey, R. E., and W. Y. Chen, 1983: Statistical field significance and its determination by Monte Carlo techniques. *Mon. Wea. Rev.,* **111,** 46–59.

Lo, F., and M. P. Clark, 2002: Relationships between spring snow mass and summer precipitation in the southwestern United States associated with the North American monsoon system. *J. Climate,* **15,** 1378–1385.

Lu, L., and W. J. Shuttleworth, 2002: Incorporating NDVI-derived LAI into the climate version of RAMS and its impact on regional climate. *J. Hydrometeor.,* **3,** 347–362.

Mann, M. E., and J. Park, 1994: Global scale modes of surface temperature variability on interannual to century time scales. *J. Geophys. Res.,* **99,** 25 819–25 833.

——, and ——, 1996: Joint spatiotemporal modes of surface temperature and sea level pressure variability in the Northern Hemisphere during the last century. *J. Climate,* **9,** 2137–2162.

Mantua, N. J., S. R. Hare, U. Zhang, J. M. Wallace, and R. C. Francis, 1997: A Pacific interdecadal climate oscillation with impacts on salmon production. *Bull. Amer. Meteor. Soc.,* **78,** 1069–1079.

Matsui, T., V. Lakshmi, and E. E. Small, 2005: The effects of satellite-derived vegetation cover variability on simulated land–atmosphere interactions in the NAMS. *J. Climate,* **18,** 21–40.

McKee, T. B., N. J. Doesken, and J. Kleist, 1999: Historical dry and wet periods in Colorado. Climatology Rep. 99-1, Part A: Tech. Rep., Department of Atmospheric Science, Colorado State University, 121 pp.

McNider, R. T., and R. A. Pielke Sr., 1981: Diurnal boundary-layer development over sloping terrain. *J. Atmos. Sci.,* **38,** 2198–2212.

Mears, C. A., M. C. Schabel, and F. J. Wentz, 2003: A reanalysis of the MSU Channel 2 tropospheric temperature record. *J. Climate,* **16,** 3650–3664.

Mesinger, F., and Coauthors, 2006: North American regional reanalysis. *Bull. Amer. Meteor. Soc.,* **87,** 343–360.

Mo, K. C., and J. N. Paegle, 2000: Influence of sea surface temperature anomalies on the precipitation regimes over the southwest United States. *J. Climate,* **13,** 3588–3598.

——, and E. H. Berbery, 2004: Low-level jets and summer precipitation regimes over North America. *J. Geophys. Res.,* **109,** D06117, doi:10.1029/2003JD004106.

——, J. N. Paegle, and R. W. Higgins, 1997: Atmospheric processes associated with summer floods and droughts in the central United States. *J. Climate,* **10,** 3028–3046.

Newman, M., and P. D. Sardeshmukh, 1998: The impact on the North Pacific/North American response to remote low-frequency forcing. *J. Atmos. Sci.,* **55,** 1336–1353.

North, G. R., T. L. Bell, R. F. Cahalan, and F. J. Moeng, 1982: Sampling errors in the estimation of empirical orthogonal functions. *Mon. Wea. Rev.,* **110,** 699–706.

Pal, J. S., and E. A. B. Eltahir, 2001: Pathways relating soil moisture conditions to future summer rainfall with a model of the land–atmosphere system. *J. Climate,* **14,** 1227–1242.

——, and ——, 2003: A feedback mechanism between soil moisture distribution and storm tracks. *Quart. J. Roy. Meteor. Soc.,* **129,** 2279–2297.

Philander, S. G. H., and D. Gu, 1997: Interdecadal climate fluctuations that depend on exchanges between the Tropics and extratropics. *Science,* **275,** 805–807.

Pielke, R. A., Sr., 2001: Influence of the spatial distribution of vegetation and soils on the prediction of cumulus convective rainfall. *Rev. Geophys.,* **39,** 151–177.

——, and Coauthors, 2005: Drought 2002 in Colorado—An unprecedented drought or a routine drought? *Pure Appl. Geophys.,* **162,** 1455–1479.

Rajagopalan, B., M. E. Mann, and U. Lall, 1998: A multivariate frequency-domain approach to long-lead climate forecasting. *Wea. Forecasting,* **13,** 58–74.

Reynolds, R. W., and T. M. Smith, 1994: Improved global sea surface temperature analyses using optimum interpolation. *J. Climate,* **7,** 929–948.

Richman, M. B., 1986: Review article: Rotation of principal components. *J. Climatol.,* **6,** 293–335.

Rodwell, M. J., and B. J. Hoskins, 2001: Subtropical anticyclones and summer monsoons. *J. Climate,* **14,** 3192–3211.

Saleeby, S. M., and W. R. Cotton, 2004: Simulations of the North American monsoon system. Part I: Model analysis of the 1993 monsoon season. *J. Climate,* **17,** 1997–2018.

Sardeshmukh, P. D., and B. J. Hoskins, 1988: The generation of global rotational flow by steady idealized tropical divergence. *J. Atmos. Sci.,* **45,** 1228–1251.

Schneider, N., and B. D. Cornuelle, 2005: The forcing of the Pacific decadal oscillation. *J. Climate,* **18,** 4355–4373.

Schubert, S. D., M. J. Suarez, P. J. Pegion, and M. A. Kistler, 2002: Predictability of zonal means during boreal summer. *J. Climate,* **15,** 420–434.

——, ——, ——, R. D. Koster, and J. T. Bacmeister, 2004: Causes of long-term drought in the U.S. Great Plains. *J. Climate,* **17,** 485–503.

Seager, R., and Coauthors, 2004: Predicting Pacific decadal variability. *Earth Climate,* C. Wang, S.-P. Xie, and J. A. Carton, Eds., Amer. Geophys. Union, 105–120.

Small, E. E., 2001: The influence of soil moisture anomalies on variability of the North American monsoon system. *Geophys. Res. Lett.,* **28,** 139–142.

Sutton, R. T., and D. L. R. Hodson, 2005: Atlantic Ocean forcing of North American and European summer climate. *Science,* **309,** 115–118.

Ting, M., and H. Wang, 1997: Summertime U.S. precipitation variability and its relation to Pacific sea surface temperature. *J. Climate,* **10,** 1853–1873.

Trenberth, K. E., and G. W. Branstator, 1992: Issues in establishing the 1988 drought over North America. *J. Climate,* **5,** 159–172.

Wang, W., and A. Kumar, 1998: A GCM assessment of atmospheric seasonal predictability associated with soil moisture anomalies over North America. *J. Geophys. Res.,* **103,** 28 637–28 646.

Zhang, Y., J. M. Wallace, and D. S. Battisti, 1997: ENSO-like interdecadal variability: 1900–93. *J. Climate,* **10,** 1004–1020.

Zhu, C., D. P. Lettenmaier, and T. Cavazos, 2005: Role of antecedent land surface conditions on North American monsoon rainfall variability. *J. Climate,* **18,** 3104–3121.